On Natural Modes in Two-dimensional Asymmetric and Symmetric Moonpools in Finite Water Depth

Haiyang Huang,* Xinshu Zhang,†

State Key Laboratory of Ocean Engineering and CISSE, Shanghai Jiao Tong University, Shanghai 200240, China

1   Introduction

'Moonpools' are vertical openings, through the deck and hull of ships or offshore oil and gas exploration platform, used for marine and offshore operations such as pipe laying, riser hang off or diver recovery. Being exposed to incident waves or harmonic ship motions, the fluid inside moonpools may perform significant resonant motions. The resonance modes consist in sloshing modes and piston mode, where the entrapped water heaves up and down more or less like a solid. Similar fluid behavior may happen between the hulls of multi-hull vessels or between ships in a side-by-side arrangement, which can be treated as a two-dimensional moonpool (see Fig. 1). Since the large fluid motions inside moonpools may cause negative impacts, it is important to predict the resonance frequencies and modal shapes at the concept design phase.

Molin (2001) developed an ingenious method to solve the moonpool problem, based on the assumption that the water depth is infinite and the beams are very large. A series of formulations have been derived to predict the resonance frequencies. However, the results by this method may be not accurate for the case in finite water depth. Based on the domain-decomposition scheme, Faltinsen *et al.* (2007) carried out theoretical computations on the piston-like steady-state fluid motions in a two-dimensional symmetric moonpools and compared with the experimental data from model test. The predicted resonance frequencies agree well with experiments. By using this method, the fluid domain have to be divided into several subdomains and continuity condition have to be matched at the common boundaries, which may require extensive computations. Zhang & Bandyk (2013, 2014) studied the moonpool resonance for two heaving rectangular bodies in a two-layer fluid, using an eigenfunction matching approach. Based on a higher-order boundary element method, Ning *et al.* (2015, 2018) developed a fully nonlinear two-dimensional numerical wave flume to investigate the gap resonance. More recently, Molin *et al.* (2018) applied a new model to study three-dimensional moonpool/gap resonance in finite water depth and the solutions have been improved significantly comparing to the previous model.

In the present study, we developed a model to predict the resonance frequencies for two-dimensional asymmetric and symmetric moonpools in finite water depth. The objective is to develop an accurate model for estimation of the natural frequencies for asymmetric and symmetric moonpools, while keep less complicated computations.

2   Theory and Approach

The natural frequency and modes of a two-dimensional moonpool are studied by applying a theoretical model, which is illustrated in Fig. 1. The beams of the two bodies are b_1 and b_2, respectively. The draft of the two bodies are d_1 and d_2, respectively. Moonpool, with width being a, is formed between the two bodies. The water depth is h. The coordinate system is set at the lower left side of the moonpool as illustrated in the sketch. The fluid domain is divided into three subdomains. The domain decomposition is also illustrated in Fig. 1. At $x = -b_1$ and $x = a + b_2$, the outer boundaries of subdomain II and subdomain III, boundary condition $\varphi = 0$ is applied (φ is the spatial velocity potential). The velocity potential in three subdomains are denoted by φ_1, φ_2 and φ_3, respectively.
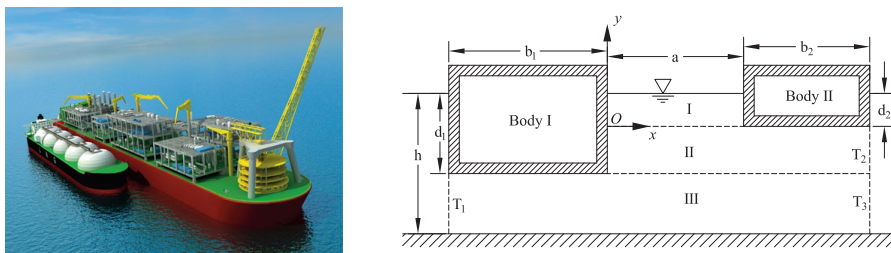

Figure 1: Side-by side offloading (Left). Sketch of the problem and coordinate system (Right).

*Presenting author

†Corresponding author (xinshuz@sjtu.edu.cn)

The natural modes are eigen solutions of the following boundary value problem

$$\Delta\varphi_1 = 0 \tag{1}$$

$$\Delta\varphi_2 = 0 \tag{2}$$

$$\Delta\varphi_3 = 0 \tag{3}$$

Free surface boundary condition:
$$\frac{\partial\varphi_1}{\partial y} = \frac{\omega^2}{g}\varphi_1 \qquad 0 \le x \le a \qquad y = d_2 \tag{4}$$

Wall boundary condition:
$$\frac{\partial\varphi_1}{\partial x} = 0 \qquad (x = 0) \,\&\, (x = a) \qquad 0 \le y \le d_2 \tag{5}$$

Body bottom boundary condition:
$$\frac{\partial\varphi_2}{\partial y} = 0 \qquad a \le x \le a + b_2 \qquad y = 0 \tag{6}$$

Wall boundary condition:
$$\frac{\partial\varphi_2}{\partial x} = 0 \qquad x = 0 \qquad d_2 - d_1 \le y \le 0 \tag{7}$$

Truncated boundary condition:
$$\varphi_2 = 0 \qquad x = a + b_2 \qquad d_2 - d_1 \le y \le 0 \tag{8}$$

Body bottom boundary condition:
$$\frac{\partial\varphi_3}{\partial y} = 0 \qquad -b_1 \le x \le 0 \qquad y = d_2 - d_1 \tag{9}$$

Seabed boundary condition:
$$\frac{\partial\varphi_3}{\partial y} = 0 \qquad -b_1 \le x \le a + b_2 \qquad y = d_2 - h \tag{10}$$

Truncated boundary condition:
$$\varphi_3 = 0 \qquad (x = -b_1) \,\&\, (x = a + b_2) \qquad d_2 - h \le y \le 0 \tag{11}$$

The velocity potentials for subdomain I, II and III can be written as

$$\varphi_1 = A_0 + B_0\frac{y}{d_2} + \sum_{n=1}^{\infty}[A_n\cosh(k_n y) + B_n\sinh(k_n y)]\cos(k_n x) \tag{12}$$

$$\varphi_2 = \sum_{n=1}^{\infty}[C_n\cosh(\mu_n y) + D_n\sinh(\mu_n y)]\cos(\mu_n x) \tag{13}$$

$$\varphi_3 = \sum_{n=1}^{\infty}E_n\frac{\cosh(\lambda_n(y + h - d_2))}{\cosh(\lambda_n(h - d_1))}\sin(\lambda_n(x + b_1)) \tag{14}$$

where $k_n = n\pi/a$, $\mu_n = \pi(n - 1/2)/(a + b_2)$ and $\lambda_n = n\pi/(a + b_1 + b_2)$.
Match φ_1 and φ_2, we obtain

$$\varphi_2 = \varphi_1 \qquad 0 \le x \le a \qquad y = 0 \tag{15}$$

and

$$\frac{\partial\varphi_2}{\partial y} = \begin{cases} \dfrac{\partial\varphi_1}{\partial y} & 0 \le x \le a & y = 0 \\[2mm] 0 & a < x \le a + b_2 & y = 0 \end{cases} \tag{16} \tag{17}$$

Match φ_2 and φ_3, we obtain

$$\varphi_3 = \varphi_2 \qquad 0 \le x \le a + b_2 \qquad y = d_2 - d_1 \tag{18}$$

and

$$\frac{\partial\varphi_3}{\partial y} = \begin{cases} \dfrac{\partial\varphi_1}{\partial y} & 0 \le x \le a + b_2 & y = d_2 - d_1 \\[2mm] 0 & -b_1 < x \le a & y = d_2 - d_1 \end{cases} \tag{19} \tag{20}$$

Combine (4) and (12), we obtain

$$\frac{B_0}{d_2} = \frac{\omega^2}{g}(A_0 + B_0) \tag{21}$$

$$k_n A_n\tanh k_n d_2 + k_n B_n = \frac{\omega^2}{g}(A_n + B_n\tanh k_n d_2) \tag{22}$$

which can be written as the vectorial equation

$$\mathbf{M_1}\cdot\vec{A} + \mathbf{M_2}\cdot\vec{B} = \frac{\omega^2}{g}(\vec{A} + \mathbf{M_3}\cdot\vec{B}) \tag{23}$$

with $\mathbf{M_1}, \mathbf{M_2}, \mathbf{M_3}$ diagonal matrices, which are written as

$$\text{diag }\mathbf{M_1} = (0, k_n\tanh k_n d_2) \tag{24}$$

$$\text{diag }\mathbf{M_2} = (1/d_2, k_n) \tag{25}$$

$$\text{diag }\mathbf{M_3} = (1, \tanh k_n d_2) \tag{26}$$

Combine (12), (13) and (15), and integrate each side with 1, $\cos(k_1 x)$, $\cos(k_2 x)$ ... , we obtain

$$A_0 = \sum_{n=1}^{\infty} \frac{C_n}{a\mu_n} \sin(\mu_n a) \tag{27}$$

$$A_m = \sum_{n=1}^{\infty} \frac{C_n}{a} \left[\frac{\sin((k_m - \mu_n)a)}{k_m - \mu_n} - \frac{\sin((k_m + \mu_n)a)}{k_m + \mu_n} \right] \tag{28}$$

which can be written as the vectorial equation

$$\overrightarrow{A} = \mathbf{AC} \cdot \overrightarrow{C} \tag{29}$$

Combine (12), (13), (16) and (17), and integrate each side with $\cos(\mu_1 x)$, $\cos(\mu_2 x)$, $\cos(\mu_3 x)$ ... , we obtain

$$D_m = \frac{2B_0}{\mu_m^2 d_2 (a + b_2)} + \sum_{n=1}^{\infty} \frac{k_n B_n}{\mu_m (a + b_2)} \left[\frac{\sin((\mu_m - k_n)a)}{\mu_m - k_n} - \frac{\sin((\mu_m + k_n)a)}{\mu_m + k_n} \right] \tag{30}$$

which can be written as the vectorial equation

$$\overrightarrow{D} = \mathbf{DB} \cdot \overrightarrow{B} \tag{31}$$

Combine (13), (14) and (18), and integrate each side with $\cos(\mu_1 x)$, $\cos(\mu_2 x)$, $\cos(\mu_3 x)$ ... , we obtain

$$C_m + D_m \tanh((d_2 - d_1)\mu_m) = \sum_{n=1}^{\infty} \frac{E_n}{(a + b_2)\cosh((d_1 - d_2)\mu_m)} \cdot$$
$$\left[\frac{\cos((\mu_m - \lambda_n)(a + b_2) - \lambda_n b_1) - \cos(\lambda_n b_1)}{\mu_m - \lambda_n} - \frac{\cos((\mu_m + \lambda_n)(a + b_2) + \lambda_n b_1)}{\mu_m + \lambda_n} \right] \tag{32}$$

which can be written as the vectorial equation

$$\overrightarrow{C} + \mathbf{M_4} \cdot \overrightarrow{D} = \mathbf{CDE} \cdot \overrightarrow{E} \tag{33}$$

with $\mathbf{M_4}$ diagonal matrices, which are written as

$$\operatorname{diag} \mathbf{M_4} = \tanh((d_2 - d_1)\mu_n) \tag{34}$$

Combine (13), (14), (19) and (20), and integrate each side with $\sin(\lambda_1(x + b_1))$, $\sin(\lambda_2(x + b_1))$, $\sin(\lambda_3(x + b_1))$ ... , we obtain

$$E_m = \sum_{n=1}^{\infty} \frac{\mu_n \cosh(\mu_n(d_1 - d_2))}{\lambda_m \tanh(\lambda_m(h - d_1))(a + b_1 + b_2)} \left[C_n \tanh((d_2 - d_1)\mu_n)) + D_n \right] \cdot$$
$$\left[\frac{\cos((\mu_n - \lambda_m)(a + b_2) - \lambda_m b_1) - \cos(\lambda_m b_1)}{\mu_n - \lambda_m} - \frac{\cos((\mu_n + \lambda_m)(a + b_2) + \lambda_m b_1) - \cos(\lambda_m b_1)}{\mu_n + \lambda_m} \right] \tag{35}$$

which can be written as the vectorial equation

$$\overrightarrow{E} = \mathbf{ECD} \cdot (\mathbf{M_4} \cdot \overrightarrow{C} + \overrightarrow{D}) \tag{36}$$

By combing (29), (31), (33) and (36), it yields

$$\overrightarrow{A} = \mathbf{AC} \cdot (\mathbf{CDE} \cdot \mathbf{ECD} \cdot \mathbf{M_4} - \mathbf{I})^{-1} \cdot (\mathbf{M_4} - \mathbf{CDE} \cdot \mathbf{ECD}) \cdot \mathbf{DB} \cdot \overrightarrow{B} = \mathbf{AB} \cdot \overrightarrow{B} \tag{37}$$

where $\mathbf{I}$ is the unit matrix.

Combine (23) and (37), we get

$$(\mathbf{AB} + \mathbf{M_3})^{-1}(\mathbf{M_1} \cdot \mathbf{AB} + \mathbf{M_2}) \cdot \overrightarrow{B} = \frac{\omega^2}{g} \overrightarrow{B} \tag{38}$$

When the series (12) is truncated to some order N, the numerical resolutions of the eigen-value problem (38) yield the natural frequencies and the associated modal shapes of the free surface. Numerical convergence has been assessed by repeating the computations for increasing values of N.

We remark that the present model works for asymmetric moonpool formed by two bodies with different sizes. But the formulation has also been simplified for a symmetric moonpool configuration. A so-called simplified mode approximation (SMA) of the piston mode has been derived for the symmetric case, and can be used for rapid estimation of the resonance frequency of piston mode.
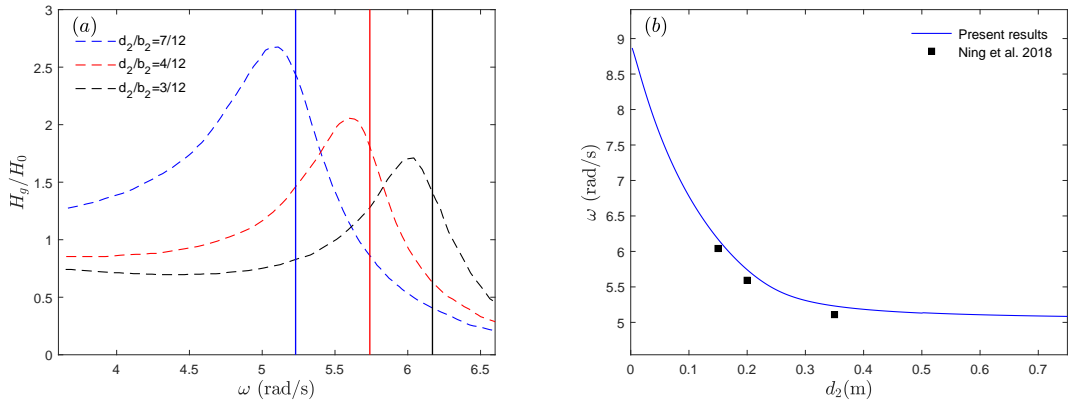
Figure 2: (a)Variation of wave elevation inside moonpool with respect to body draft d_2 for $b_1 = b_2 = 0.6$ m, $a = 0.06$ m, $d_1 = 5/12b_2$, $h = 1$ m. The dashed line: results by Ning *et al.* (2018). The solid lines: present results on natural frequency (piston mode); (b) Variation of piston mode frequencies with respect to the draft of body II.
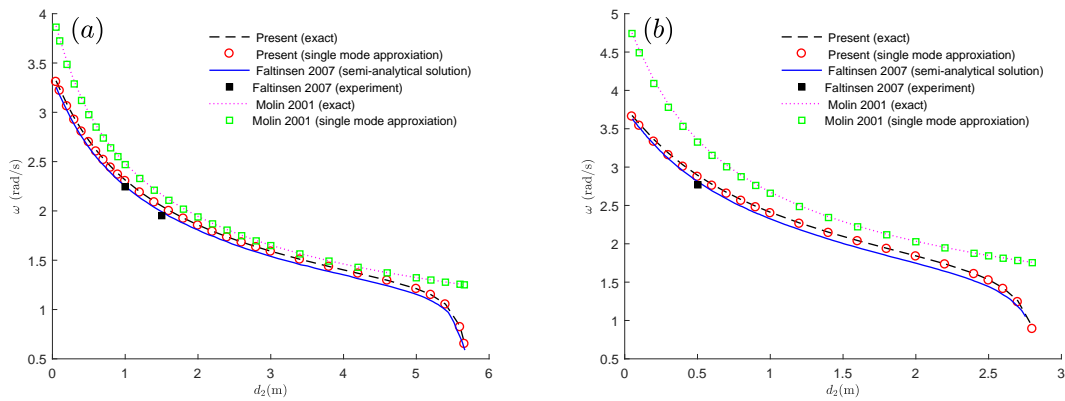

Figure 3: Comparison of the piston mode resonance frequencies with the experiments and other solutions. Variation of natural frequency with respect to the draft $d_1 = d_2$. Two cases are computed: (a) $b_1 = b_2 = 2$ m, $a = 1$ m, $h = 5.72222$ m; (b) $b_1 = b_2 = 1$ m, $a = 1$ m, $h = 2.86111$ m.

3   Results and Discussion

The present asymmetric model has been validated by comparing to the numerical results by Ning *et al.* (2018). As show in Fig. 2(a), the present prediction of the piston mode resonance frequency agree well with the solutions by the boundary element code for three different asymmetry moonpool configurations. Fig. 2(b) presents the effects of draft of body II on the piston mode frequencies.

Two-dimensional symmetric moonpool has also been tested. Both exact solution and single mode approximation are presented. Fig. 3 illustrate the comparison of the predicted natural frequencies using present model with experiments and numerical results by the other models. The piston mode frequencies are plotted with respect to the draft of the body. As can be observed, the present results agree well the experimental results and semi-analytical results by Faltinsen *et al.* (2007). In addition, the solutions using present models (both exact and SMA) have been improved comparing the model by Molin (2001). As also can be seen, the piston mode resonance frequency decrease as the draft increases. More results and detailed analyses will be presented at the workshop.

References

FALTINSEN, O. M., ROGNEBAKKE, O. F. & TIMOKHA, A. N. 2007 Two-dimensional resonant piston-like sloshing in a moonpool. *J. Fluid Mech.* **575**, 359–397.

MOLIN, B. 2001 On the piston and sloshing modes in moonpools. *J. Fluid Mech.* **430** (5), 27–50.

MOLIN, B., ZHANG, X., HUANG, H. & REMY, F. 2018 On natural modes in moonpools and gaps in finite depth. accepted. *J. Fluid Mech.* .

NING, D., SU, X., ZHAO, M. & TENG, B. 2015 Numerical study of resonance induced by wave action on multiple rectangular boxes with narrow gaps. *Acta Oceanol. Sin.* **34** (5), 92–102.

NING, D., ZHU, Y., ZHANG, C., ZHAO, M. & TENG, B. 2018 Influences of body draught on water resonance at a gap between two identical barges. submitted.

ZHANG, X. & BANDYK, P. 2013 On two-dimensional moonpool resonance for twin bodies in a two-layer fluid. *Appl. Ocean Res.* **40**, 1–13.

ZHANG, X. & BANDYK, P. 2014 Two-dimensional moonpool resonances for interface and surface-piercing twin bodies in a two-layer fluid. *Appl. Ocean Res.* **47**, 204–218.